Biomaterials 232 (2020) 119683

Contents lists available at ScienceDirect

Biomaterials

journal homepage: www.elsevier.com/locate/biomaterials

Contractile myosin rings and cofilin-mediated actin disassembly orchestrate ECM nanotopography sensing

Stefania Di Cio[a,b], Thomas Iskratsch[a,b], John T. Connelly[a,c], Julien E. Gautrot[a,b,*]

[a] Institute of Bioengineering, Queen Mary, University of London, Mile End Road, London, E1 4NS, UK
[b] School of Engineering and Materials Science, Queen Mary, University of London, Mile End Road, London, E1 4NS, UK
[c] Barts and the London School of Medicine and Dentistry, Queen Mary, University of London, 4 Newark Street, London, E1 2AT, UK

ARTICLE INFO

Keywords:
Actin cytoskeleton
Nanopatterning
Nanofibres
Cofilin

ABSTRACT

The nanotopography and nanoscale geometry of the extra-cellular matrix (ECM) are important regulators of cell adhesion, motility and fate decision. However, unlike the sensing of matrix mechanics and ECM density, the molecular processes regulating the direct sensing of the ECM nanotopography and nanoscale geometry are not well understood. Here, we use nanotopographical patterns generated via electrospun nanofibre lithography (ENL) to investigate the mechanisms of nanotopography sensing by cells. We observe the dysregulation of actin dynamics, resulting in the surprising formation of actin foci. This alteration of actin organisation is regulated by myosin contractility but independent of adapter proteins such as vinculin. This process is highly dependent on differential integrin expression as β3 integrin expressing cells, more sensitive to nanopattern dimensions than β1 integrin expressing cells, also display increased perturbation of actin assembly and actin foci formation. We propose that, in β3 integrin expressing cells, contractility results in the destabilisation of nanopatterned actin networks, collapsing into foci and sequestering regulators of actin dynamics such as cofilin that orchestrate disassembly. Therefore, in contrast to the sensing of substrate mechanics and ECM ligand density, which are directly orchestrated by focal adhesion assembly, we propose that nanotopography sensing is regulated by a long-range sensing mechanism, remote from focal adhesions and mediated by the actin architecture.

1. Introduction

Cell adhesion to the extra-cellular matrix (ECM) constitutes an important determinant of cell phenotype and plays an essential role in the maintenance of stem cell niches and tissue homeostasis [1–4]. Binding of ECM proteins, glycosaminoglycans and matrix bound growth factors by cell membrane receptors such as integrins [5,6], CD44 [7] and growth factor receptors [8] are primary events in a cascade of processes that eventually result in the regulation of gene expression and cell phenotype [9,10]. In addition, cell adhesions are modulated by nanoscale physical properties of the ECM, such as the mechanical properties of the matrix [11,12], the topography [13,14] and the geometry with which adhesive ligands are presented [15–18]. In these interactions, two important principles mediate the sensing of the physical properties of the ECM by cell adhesions: the molecular clutch that regulates mechanosensing [19] and ligand clustering that is controlled by the geometry and distribution of the adhesive landscape [20,21]. In contrast, the mechanism controlling cell sensing of the nanotopography and nano- to micro-scale geometry of adhesive ligands (regulating the size and shape of adhesions rather than early recruitment and clustering of membrane receptors) remains poorly understood. Contact guidance and the impact that nanotopography has on cell adhesions is well documented [22,23]. However, owing to the homogeneity of the corresponding substrates at the nanoscale, and the high stiffness of the substrates typically studied in these contexts, the molecular clutch and clustering mechanisms cannot fully account for such behaviour. Importantly, a hallmark of the regulation of cell adhesion and spreading via the molecular clutch and receptor clustering mechanisms is the associated regulation in protein recruitment at focal adhesions [16]. In contrast, the impact of the nanoscale geometry of adhesions on cell spreading does not seem to correlate with significant changes in protein recruitment at geometrically confined adhesions [17,18]. Hence, from a biochemical point of view, nano-confined adhesions remain relatively mature (in terms of protein recruitment, phosphorylation and matrix deposition), but are unable to sustain the assembly of a stable actin cytoskeleton. In addition, although plenty of evidence links adhesion size and cellular contractile forces [11,24], more recent work does not directly correlate the two [25–27]. More generally, cell shape, adhesion

* Corresponding author. School of Materials Science and Institute of Bioengineering, Queen Mary, University of London, Mile End Road, London, E1 4NS, UK.
E-mail address: j.gautrot@qmul.ac.uk (J.E. Gautrot).

https://doi.org/10.1016/j.biomaterials.2019.119683
Received 23 July 2019; Received in revised form 22 November 2019; Accepted 12 December 2019
Available online 16 December 2019

and spreading across different lineages are typically associated with major changes in the shape and size of adhesions, as well as their number [28,29]. It is also clear that integrin expression has a profound impact on adhesion geometry and cell phenotype [30,31]. Different integrins play complementary roles in mechanotransduction. Whilst α5β1 integrins are required to strengthen adhesions to fibronectin, αvβ3 integrins regulate mechanotransduction [32]. Furthermore, β1 integrins are found in nascent adhesions at cell protrusions, independently of myosin-II activity, whilst αv integrins promote the formation of mature FAs mediating mechanosensing [33]. Overall, the mechanism via which nanotopography and nanoscale confinement of ECM ligands regulate adhesion formation, cytoskeleton assembly, cell contractility and, downstream, cell phenotype remains unclear.

Here we use a novel nanopatterning technique, electrospun nanofibre lithography [18], which allows the generation of quasi-2D fibrous nanopatterns with defined fibre diameters. We have previously reported that the cell cytoskeleton undergoes substantial changes in cells spreading on nanopatterns and that differential integrin expression plays an important role in nanotopography sensing [18]. In addition, we previously observed that, although circular nanopattern dimensions significantly impact on cytoskeleton assembly and spreading area, the recruitment of proteins associated with various stages of maturation of focal adhesion assembly was not significantly impaired [17]. We now report that fibrillar nanopattern geometry also has little impact on the recruitment of the adapter protein vinculin and that knock out of vinculin has no significant impact on cell sensing of nanopatterns geometry. Therefore, we studied in detail the processes regulating cytoskeleton assembly on fibrillar nanopatterns and identify a long-range sensing mechanism, regulated by myosin contractility and cofilin-mediated disassembly, a process highly dependent on integrin expression.

2. Materials and methods

2.1. Nanopatterning

The fibrous patterns were produced via Electrospun Nanofibre Lithography (ENL) [18]. Briefly, silicon wafers or glass slides were plasma treated for 10 min and then incubated overnight in a solution of 30 μL of 3-trimethoxysilylpropyl 2-bromo-2methyl-propionate (Fluorochem) and 50 μL of triethylamine (Sigma Aldrich) dissolved in 30 mL toluene.Poly (methyl methacrylate) (PMMA, 350000 and 996000 Mw from Sigma Aldrich) was then used to produce the electrospun nanofibres. The polymer was dissolved in a mixture of DMF (N,N-Dimethilformamide) and chloroform. PMMA was used at different concentrations and Mw depending on the fibre diameters needed. The as spun fibres were annealed for about 1 h at different temperatures depending on the fibre sizes. A monolayer of non-fouling polymer brushes was then deposited in between the fibres (poly (oligoethyleneglycol methacrylate)) with thicknesses of 60, 30 or 10 nm [34]. The PMMA fibres were then removed using chloroform, leaving a network of adhesive nanofibres to which fibronectin can be deposited to promote cell adhesion. The fibre diameters produced were: 250, 500 and 1000 nm (see Table 1). For live imaging experiments, the patterns were produced on thin glass coverslips. The resulting nanopatterned coverslips were glued to the bottom of petri dishes with an 11 nm hole previously drilled.

2.2. Cell culture and seeding

GEβ3 and GEβ1 cells (β1-deficient epithelial cells in which αvβ3 and α5β1 integrins are stably expressed) were a kind gift from Prof. Arnoud Sonnenberg. Expression levels of α5β1 and αvβ3 integrins are reported in previously published work [35,36] and we confirmed that α5β1 expressing cells did not adhere in the presence of β1 integrin function blocking antibody (P5D2 20 μg/mL, ab24693), whereas αvβ3 expressing cells adhered normally. Cells were cultured in DMEM (Thermo Fisher) supplemented with 10% FBS, glutamine and antibiotics. Cells were cultured to confluency (about 80% density) and were detached using trypsin/versene (1:9) and reseeded on either fibrous patterns or well plates.

Table 1
Conditions used for producing the different fibre diameter. Three concentrations (weight percentage of the solution) of PMMA were used and two PMMA molecular weights. Fibres were annealed according to their dimension: annealing temperature (T) is in °C. Three finale patterned fibre diameters were achieved.

PMMA concentration (wt%)	PMMA Mw (kDa)	Annealing T (°C)	Patterned Fibre Diameter (nm)
3%	996 kDa	140	250
5%	996 kDa	150	500
10%	350 kDa	170	1000

Vinculin-deficient mouse embryonic fibroblast (MEFvin$^{-/-}$) were a kind gift from Dr Christoph Ballestrem. Cells were cultured in Advanced DMEM (Thermo Fisher) supplemented with 10% FBS (Fetal Bovine Serum), glutamine and antibiotics. Cells were cultured to confluency (about 80% density) and were detached using trypsin/versene (1:9) and reseeded on fibrous patterns or in culture plastic well plate for experiments.

2.3. Cell immunostaining after seeding on the nanopatterns

After 24 h incubation on the different substrates cells were fixed with 4% paraformaldehyde (in PBS) for 10 min, permeabilized with 0.2% Triton X-100 (in PBS) for 5 min and blocked with a solution of 10% FBS and 0.25% gelatin for 1 h at room temperature. Phalloidin (1:500) was added at this stage too. Samples were then incubated with the primary antibody (1:200) for 1 h at room temperature, washed and incubated with the conjugated secondary antibody (1:1000; Alexafluor 488 or 594) and DAPI (1:1000) for 1 h at room temperature and washed again before being mounted on glass slides with Mowiol solutions.

2.4. GEβ3 and GEβ1 transfection with LifeAct for live imaging experiments

Cells were seeded overnight in 6 well plates, at a density of 100000 cells/mL (2 mL/well) for transfection. The cells were then transfected with LifeAct plasmid (actin marker for the visualization of F-actin in living cells). The amount of DNA/jetPEI used was 3 μg/4 μL. After 24 h, cells were detached using trypsin/versene and 100 μL of the cell suspension was reseeded in the prepared Petri dishes with homogenous glass substrates, coated with poly L-lysine and fibronectin, or with nanofibre patterns with width of fibres of 250, 500 and 1000 nm. Cells were imaged after 24 h spreading.

2.5. MEFvin$^{-/-}$ vinculin transfection

MEFvin$^{-/-}$ were seeded overnight in 6 well plates, at a density of 100000 cells/mL (2 mL/well). They were then transfected with three different fluorescent vinculin constructs: vinculin venus (vinculin full length), vinculin T12 (VinT12, constitutively active form of vinculin) and vinculin 880 (Vin880, lacking the vinculin tail and associated actin binding domains). 7 μg of each DNA were separately dissolved in 100 μL of a sodium chloride solution and 8 μL of the transfecting agent jetPEI (for each DNA) were diluted in 100 μL of a sodium chloride solution. The solution containing the jetPEI was then added to the DNA solution, flicked for mixing and left 15–20 min to complex. The solution was then added to the culture plate where cell medium had been replaced with optiMEM. Cells were left for 4 h to transfect, after which medium was switched back to DMEM. After 24 h from transfection, cells were detached using trypsin/versene and reseeded in 48 well

plates, on the fibrous patterns and homogenous control substrates, at a density of 15000 cells/mL and 0.5 mL/well. After 7 h of spreading, cells were fixed and stained with phalloidin and DAPI, prior to mounting and fluorescence imaging.

2.6. Inhibitors treatment

Inhibitors Y-27632 (R&D Systems) and Blebbistatin (Sigma Aldrich) were diluted in DMSO so to achieve stock solutions of 10 mM. GEβ3 and GEβ1 cells were seeded on nanofibres with different diameters in a 48 well plate, at densities of 7500 cells/mL and 0.5mL/well. After 24 h, they were treated with one of the two inhibitors for 4 h at a concentration of 10 μM in DMEM medium [37,38]. Non-treated cells were incubated in DMEM/DMSO at the same concentration used for the inhibitors. They were then fixed and stained for actin, nucleus and vinculin for cell spreading and FA characterisation. Cells were also treated with the Arp2/3 inhibitor, ck666 [39], and the formin inhibitor smiFH2 [41]. Cells were incubated for 3 h with 300 μM of ck666, 30 μM of smiFH2 [39]or DMSO as control. They were then fixed and stained for actin, nucleus and vinculin.

2.7. Cofilin and α-actinin knock-down in GEβ3

α-Actinin knock-down was carried out using Lipofectamine 2000 (Invitrogen). GEβ3 cells were seeded overnight in 6 well plates at a density of 75000 cells/mL (2 mL/well). A mixture of Lipofectamine (5 μL) and siRNA (100 pmol) in opti-MEM was then added to the plate for 4 h. Two α-actinin siRNA probes were tested targeting different sequences (Qiagen SI02742859 -ACTCGACTAACTCATACTGT- and SI00888692 - ACAACCTACG ACTCCTGTAG). A non-targeting siRNA was also used (AllStar Negative Control siRNA, Qiagen 1027280). Medium was then changed to DMEM. After 48 h, cells were detached and reseeded on nanofibrous patterns (with fibre diameters of 500 and 1000 nm) or homogenous surfaces (Ctrl) in 48 well plates at density of 10k/mL and 0.5 mL/well, allowed to spread for 4 h and then were fixed and stained for the relevant protein. For the cofilin knock-down, we used a polymer brush-based vector [42], mixed with 100 pmol siRNA (Cfl 1 siRNA, Thermo Fisher s121364 - CAGAAGTTGT GGTCTTCTTC - and s121365 - GACCATCCTC TACACCCCGT) using a similar protocol as for the Lipofectamine.

2.8. Western blot

Protein quantification. After transfection, cells were harvested (normal trypsinisation) and washed with pre warmed PBS twice. Cell pellets were then collected in Eppendorf tubes; lysis buffer was pre-cooled on ice and added to the pellets (20–80 μL depending on the total cell amount). The lysis process was carried out on ice for 1 h, using a pipet gun to mix in between to ensure the full lysis. The protein content was quantified (Pierce BCA Protein Assay Kit, Thermo-Fisher) using a standard protocol provided. Equal protein loading (20–80 μL depending on total protein concentration) was further confirmed by GAPDH.

Gel running. Bands were separated on 4–15% SDS-PAGE gradient gels (Bio-Rad) and semidry transferred onto PVDF membranes. Blots were incubated with blocking buffer (5% milk powder and 5% FBS in TBS buffer) at room temperature for 1 h before incubating with an anti-cofilin or α-actinin monoclonal antibody at 1:1000 in blocking buffer at 4 °C overnight while shaking. After washing three times with TBS + tween buffer (15 min x 3), secondary IRDye 800CW donkey anti-rabbit IgG (H + L) (1:15000, Li-cor) in blocking buffer was applied for a further 1 h incubation at room temperature. The blot was then washed with TBS + tween buffer twice for 15 min x 2 and TBS once for 15 min. Bands were visualized using an odyssey imaging system (Li-cor).

2.9. GEβ3 double transfection for live imaging

GEβ3 cells were seeded overnight in 6 well plates at a density of 100000 cells/mL (2 mL/well) for transfections. Cells were transfected with LifeAct and either myosin – GFP (Addgene plasmid # 38297) [43] or cofilin - GFP (Addgene plasmid # 50859) [44]. Lipofectamine was used by mixing 10 μL with 4 μg of each DNA plasmid. Cells were left for 4 h with the complex in Opti-MEM and then overnight in normal DMEM. Cells were then detached using trypsin/versene and 100 μL of the cell suspension was reseeded in the prepared Petri dishes, with nanofibre sizes of 500 and 1000 nm. Cells were imaged the day after.

2.10. Immuno-fluorescence microscopy and data analysis

To quantify the recruitment intensity of FAs, GEβ3 cells were seeded overnight on the nanopatterns and then stained for vinculin. 10–15 cells were analysed and experiments were carried out in triplicates. Confocal images of vinculin staining were analysed with ImageJ: images were thresholded and data extrapolation (shape descriptor and mean intensity) were performed on each object (single adhesions).

Fluorescence microscopy images of vinculin/actin staining on different brush heights and fibre dimensions and after inhibitor treatment were obtained with a Leica TCS SP2 confocal and multiphoton microscope (X-CITE 120 LED lamp, 63 × 1.4 Oil lens). Fluorescence microscopy images to quantify MEFvin$^{-/-}$ cell spreading (after phalloidin staining) were acquired with a Leica DMI 4000B epifluorescence microscope (EL6000 lamp, 20 × 0.7 NA lens, 63 × 1.40 Oil lens). To quantify MEFvin$^{-/-}$ cell area, 100–150 cells were analysed and experiments were carried out in triplicates or more. Fluorescence microscopy images to quantify GEβ3 cells spreading, shape and cell density were acquired with a Leica DMI 4000B epifluorescence microscope (EL6000 lamp, 20 × 0.7 NA lens, 63 × 1.40 Oil lens). 100 cells per condition were analysed and experiments were carried out in triplicates. For siRNA experiments, only cells that were not expressing the respective protein (α-actinin or cofilin, as assessed via immunostaining) were analysed.

2.11. Live imaging

GEβ3 and GEβ1 cells expressing LifeAct and GEβ3 cells expressing LifeAct and myosin/cofilin –GFP and seeded on either patterned surfaces or homogenous substrates were analysed for live cell microscopy with a Zeiss Super resolution LSM 710 ELYRA PS1 equipped with an environmental chamber, in which the level of CO_2 was kept at 5% and temperature at 37.5 °C. Live cell images were acquired using a 63 × 1.4NA oil DIC M27 objective in confocal mode. LifeAct fluorescence was stimulated using a 543-nm diode laser, while the respective second protein (GFP tagged) using a 488-nm diode laser. For live imaging experiments, images were collected over 150 min or 90 min for the double transfections, taking images every 1 min and 5 to 10 cells were analysed per experiments. Experiments were repeated in triplicate.

2.12. Statistical analysis

Statistical analysis was carried out using Origin 8 and one-way ANOVA with Tukey test for posthoc analysis. Significance was determined by * $P < 0.05$, ** $P < 0.01$, *** $P < 0.001$, n.s. not significant. A full summary of statistical analysis is provided in the Supplementary Tables. In figure captions, "n" means the number of independent replicates of the experiment presented.

3. Results

To investigate the impact of nano- to micro-scale confinement of adhesions on cell spreading and cytoskeleton assembly, we used

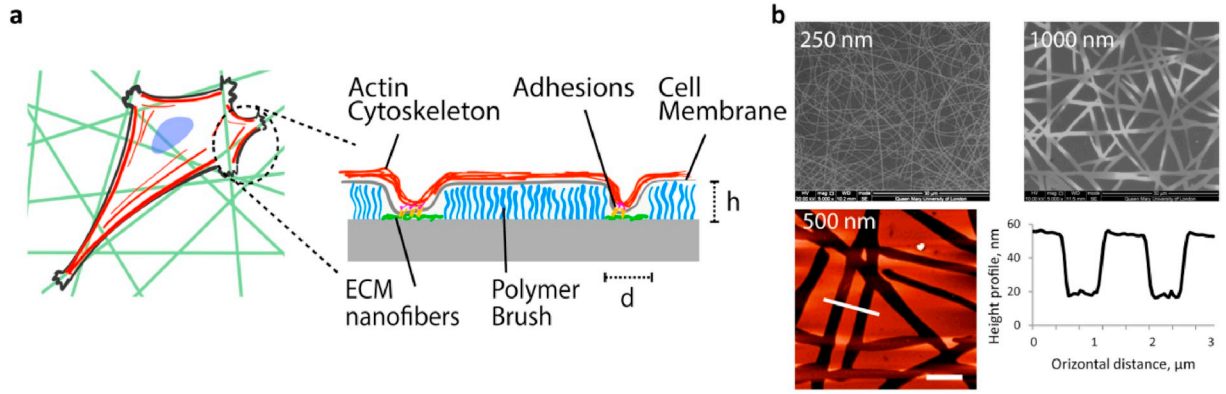

Fig. 1. Fibrous adhesive patterns generated via electrospun nanofibre lithography (ENL). a. Schematic of cell spreading on nanofibres. Zoom: schematic representation of the cell membrane in contact with nanopatterned substrates, with polymer brushes controlling the width of adhesive nanofibres (d) and the height of the non-adhesive step (h). b. Characterisation of nanofibres. SEM (Scanning Electron Microscopy) images (top) of 250 and 1000 nm fibre diameter. AFM (Atomic Force Microscopy- bottom) of 500 nm fibres with height profile. Scale bar, 2 µm.

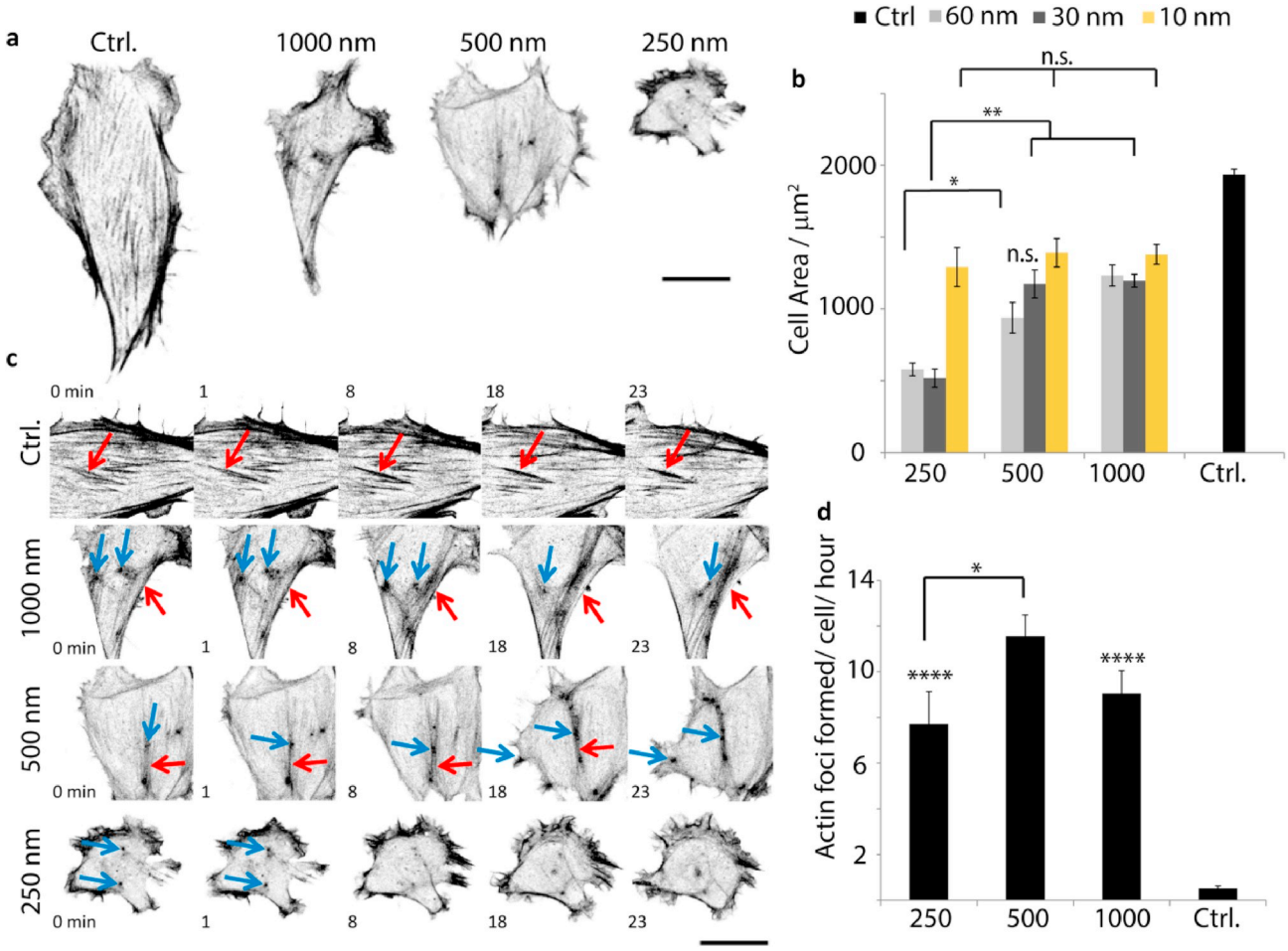

Fig. 2. The regulation of cell adhesion by nanopatterns correlates with the occurrence of actin foci. a. Images of the actin cytoskeleton of cells spreading on nanopatterned substrates. GEβ3 cells were transfected with LifeAct for these experiments. Scale bar is 20 µm. b. Cell spreading is impacted by nanofibre width (250, 500 and 1000 nm) and anti-adhesive background height (10, 30 and 60 nm). c. Time lapse images (see Supplementary Videos 1–4) of cells spreading on nanopatterned substrates and showing increasingly disrupted actin stress fibres as a function of nanopattern size (red arrows) and the formation of actin foci when spreading on nanopatterns (blue arrows). d. Quantification of the occurrence of actin foci on nanopatterned substrates. Error bars are s.e.m., $n \geq 3$; at least 100 cells for each replicate for each condition; **, $P < 0.01$; ****, $P < 0.00001$; n.s., not significant; see Supplementary Tables 1 and 2 for statistical analysis.

electrospun nanofibre lithography (ENL) [18]. This technique consists in using a sparse matt of electrospun nanofibres to protect defined areas from the growth of a highly protein resistant polymer brush, prior to release of the fibres by dissolution. The resulting pattern can be generated on large areas readily and does not introduce optical artefacts, therefore allowing high resolution live imaging of cell adhesion on nanopatterns [18]. Overall, nanofibrous patterns with controlled fibre diameters in the range of 250–1000 nm and brush heights in the range of 10–60 nm (and above) can be generated using this approach (Fig. 1a/b).

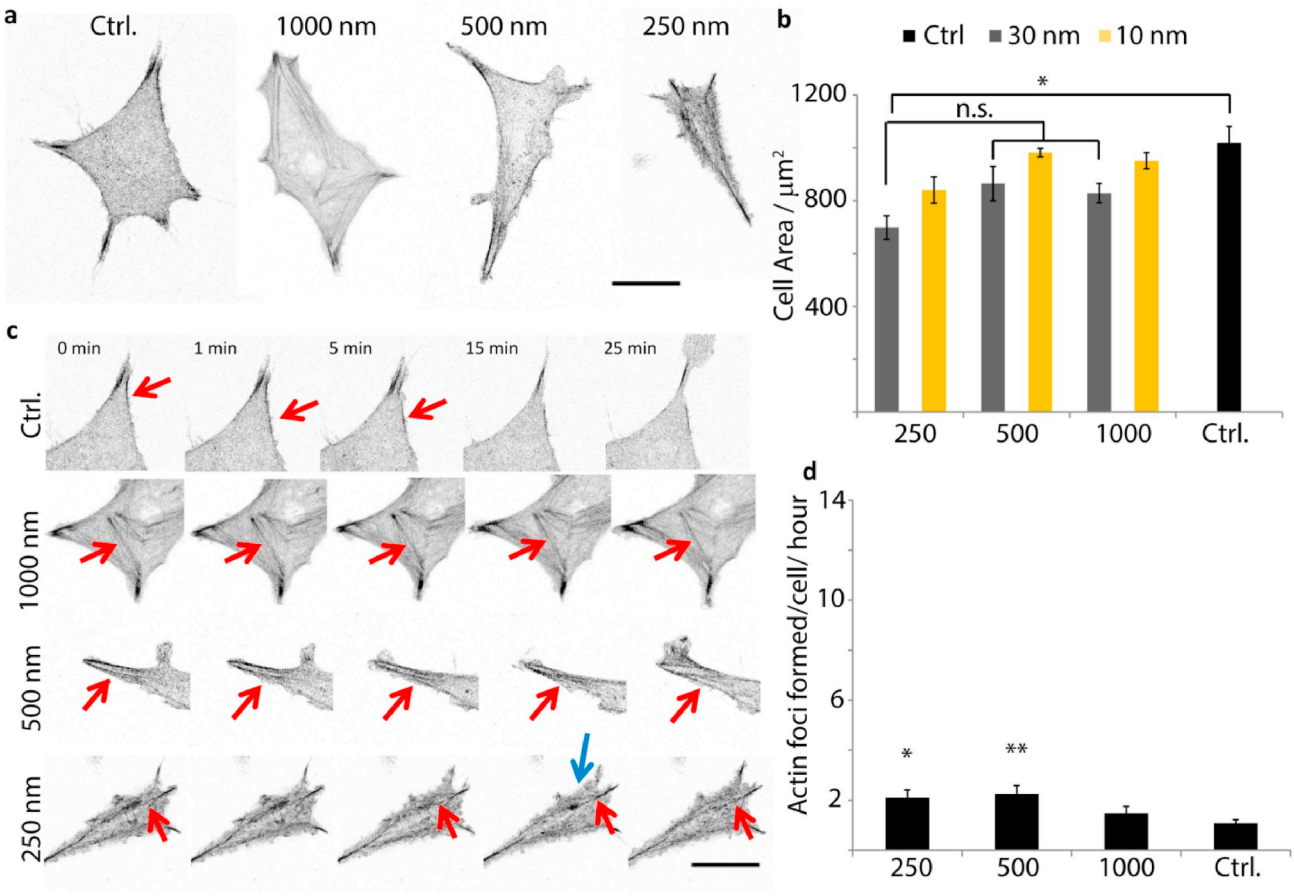

Fig. 3. GEβ1 cells display a reduced response to nanofibre diameter. a. Images of the actin cytoskeleton of GEβ1 cells (transfected with LifeAct) spreading on nanopatterned substrates. Scale bars are 20 µm. b. The response of cell spreading to nanofibre width (250, 500 and 1000 nm) and anti-adhesive background height (10 and 30 nm) is reduced compared to that of GEβ3 cells (see Fig. 2). c. Time lapse images (see Supplementary Videos 5-8) of GEβ1 cells spreading on nanopatterned substrates. Cytoskeleton assembly and stress fibre (red arrows) stabilisation is perturbed, although still present on the thinnest nanofibres (250 nm), in contrast to GEβ3 cells. Very few actin foci are observed for GEβ1 cells on all nanopatterns (blue arrows). d. Quantification of the occurrence of actin foci on nanopatterned substrates. Comparisons are with the Ctrl condition. Error bars are s.e.m., $n \geq 3$; at least 100 cells for each replicate for each condition; **, $P < 0.01$; ****, $P < 0.00001$; n.s., not significant; see Supplementary Tables 3 and 4 for statistical analysis. (For interpretation of the references to colour in this figure legend, the reader is referred to the Web version of this article.)

The spreading of GEβ3 cells (a cell line established from β1-null mouse embryos after clonal culture and selection, followed by expression of β3 integrins [29,45]) was found to be gradually restricted by the decrease in the diameter of adhesive nanofibres (fibronectin coated, Fig. 2a/b). We observed a decrease in cell spreading when comparing cell areas on 1000 nm nanofibres with cells spreading on homogenous substrates, perhaps due to the overall decrease in ECM area. The ECM area was kept constant (20%) for all nanofibrous substrates. This effect was dependent on the brush height, as thin brushes (10 nm dry thickness) did not induce a further restriction in cell spreading (although adhesions were still clearly patterned and fibrillar, Fig. 2b and Supplementary Fig. S1). Similar cell response was observed for 30 and 60 nm brushes. This suggests that the topography of the substrates, defined by the brush height, is a key feature combining to matrix geometry to regulate nanoscale sensing. We used 30 nm thick brushes for subsequent experiments.

https://doi.org/10.1016/j.biomaterials.2019.119683

In agreement with the decrease in cell spreading, the cytoskeleton of cells adhering to nanopatterns appeared more disrupted than on controls and very few stress fibres were observed on 250 nm nanofibres (Fig. 2a). To gain further insight into the mechanisms regulating the assembly of the actin cytoskeleton, we monitored actin assembly using LifeAct (Fig. 2c/d and Supplementary Videos 1–4). The dynamics of stress fibre assembly and disassembly was significantly perturbed on nanofibres, and cells spreading on 250 nm nanofibres displayed very few stress fibres. Membrane activity was also more dynamic and less persistent on nanofibres. In addition, we observed the formation of distinct actin foci arising at junctions between stress fibres, preceding their collapse and disassembly (Supplementary Videos 1-4). Very few foci were observed for cells spreading on homogenous control substrates and this number significantly increased on 1000 and 500 nm fibres, before decreasing for 250 nm (Fig. 2d). However, the number of foci formed on 250 nm fibres is likely underestimated as very few stress fibres originated from lamellipodia of cells spreading on these substrates and foci forming within the corresponding perturbed lamellipodia were difficult to distinguish from the associated dense actin network. The observation of these foci, together with the abnormal membrane activity and actin assembly, suggested that nano- to microscale confinement of adhesions is a direct regulator of actin assembly and dynamics.

In comparison, GEβ1 cells (cell line established from the same β1-null mouse embryos after clonal culture and selection, followed by expression of β1 integrins [29,45]) present very different cytoskeleton organisation (Fig. 3a) and focal adhesion shapes [18]. Cell spreading was less affected by the fibre diameter and brush height (Fig. 3b), with significant differences noticeable only between cells spreading on homogenous and the smallest patterns (250 nm). This is consistent with our previous observations that cell response to nanopattern size is

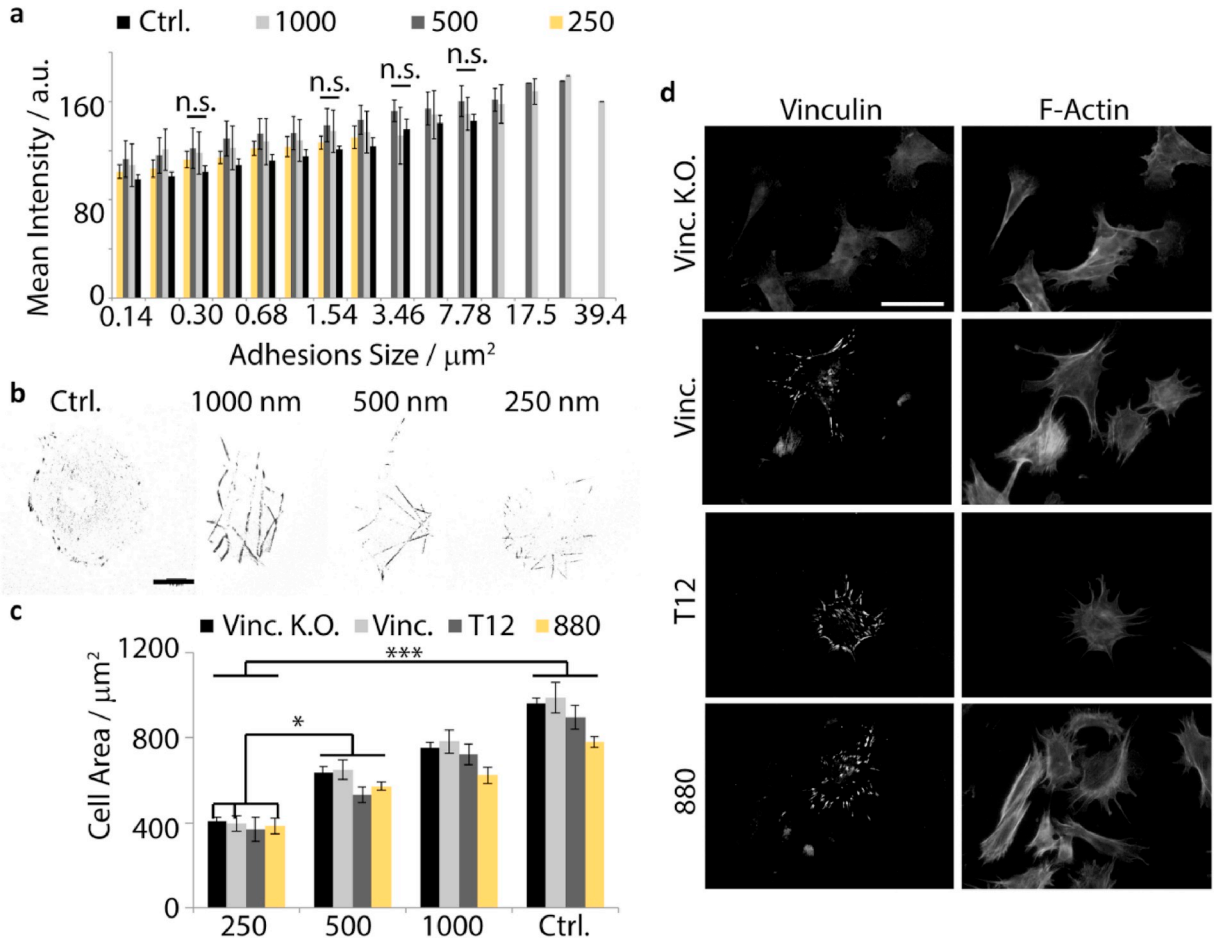

Fig. 4. Vinculin is not a key regulator of nanotopography sensing. a. Vinculin recruitment as a function of adhesion size for different nanopatterned substrates. b. Corresponding representative images of vinculin staining. Scale bar is 20 μm. c. Impact of vinculin KO on cell response to matrix nanotopography, and after re-expression of vinculin constructs (Vinc.) and dominant negative (Vin880) or constitutively active constructs (VinT12). d. Corresponding vinculin and phalloidin images. Scale bar is 50 μm. Error bars are s.e.m., $n \geq 3$; at least 100 cells for each replicate for each condition; *, $P < 0.05$; ***, $P < 0.001$; n.s., not significant; see Supplementary Tables 5 and 6 for statistical analysis.

regulated by the differential expression of integrin heterodimers [18]. Stress fibres, although perturbed, were still visible on GEβ1 cells spreading on 250 nm nanofibres. However, similarly to GEβ3 cells, GEβ1 cells seeded on patterned defined by 10 nm brushes also displayed little response to the nanopatterns width. The formation of actin foci observed for GEβ3 cells was significantly reduced in GEβ1 cells (Fig. 3c/d and Supplementary Videos 5–8), and the persistence of these foci was reduced.

https://doi.org/10.1016/j.biomaterials.2019.119683

In order to probe the role of focal adhesion assembly on this process, we first examined the adhesions formed by GEβ3 cells on nanofibres. We observed that on 1000 and 500 nm fibres, cells formed significantly larger adhesions than on homogenous substrates (Fig. 4a/b). In addition, the recruitment of focal adhesion proteins such as vinculin was not impaired on nanofibres, compared to homogenous substrates, even on 250 nm fibres, in agreement with previous observations made on circular adhesive nanopatterns [17]. Vinculin is an essential adapter protein recruited by talin, in particular during mechanical reinforcement of adhesions, providing a direct link with the actin network [46]. To further probe the role of vinculin in the regulation of nanopattern sensing, we studied the spreading of mouse embryonic fibroblasts lacking the expression of vinculin, and expressing vinculin mutants VinT12 and Vin880 [47,48] (Fig. 4c/d and Supplementary Fig. S2). The spreading of cells expressing the constitutively active VinT12, in which the head-tail association is inhibited [49], and that of cells expressing the dominant negative Vin880 [50], lacking the actin binding tail domain, displayed an essentially identical response to the nanopattern size compared to cells expressing vinculin full length. Hence the recruitment of vinculin, a key adapter protein responsible for the sensing of mechanical properties of the cell microenvironment, does not mediate the sensing of nanoscale topography and geometry.

Adapter proteins recruited at focal adhesions, such as vinculin and talin, provide a direct link between ECM bound integrins and the actin cytoskeleton, slowing down actin flow and harnessing some of the associated shear forces to establish tension and sustain membrane deformation. However, actin polymerisation, flow and stabilisation are also regulated upstream and downstream of focal adhesion-actin complexes. Arp2/3 nucleates actin polymerisation at the edge of the lamellipodium and regulates the formation of a branched actin gel in the lamella, therefore controlling membrane activity [51]. Treatment with the Arp2/3 inhibitor ck666 [40] led to a slight increase in spreading of GEβ3 cells adhering to the smallest nanopatterns (Fig. 5a and Supplementary Fig. S3). This was associated with a less polarised cell geometry, in contrast to the striking impact that fibrillar nanopatterns have on cell morphology. However, overall, cell spreading remained affected by the width of nanofibres. Similarly, perturbation of formin assembly with smifH2 [41] and knock down of α-actinin, two proteins associated with the crosslinking and stabilisation of actin bundles [52], resulted in an increase in cell areas on the thinnest nanofibres and an overall reduction of cell sensitivity to the size of nanopatterns (Fig. 5a–d and Supplementary Figs. S3 and S4). Hence, regulators of actin assembly were found to impact cell sensing of matrix

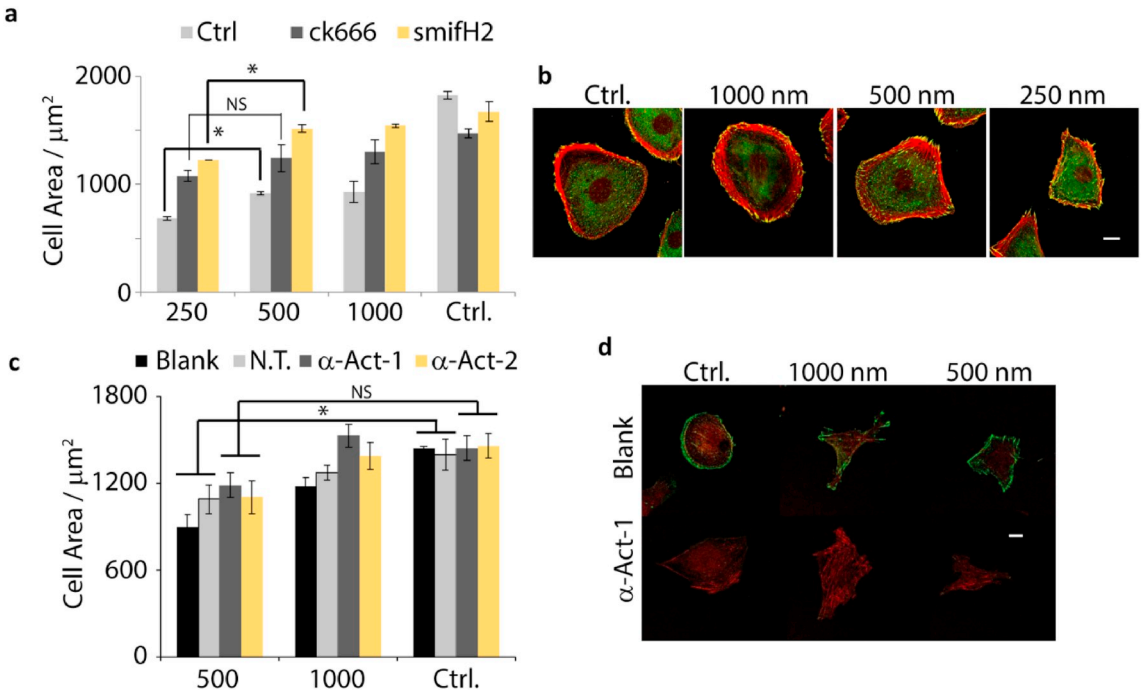

Fig. 5. Actin dynamics, rather than focal adhesion stabilisation, regulates nanotopography sensing. a. Response of GEβ3 cells treated with the inhibitors of Arp2/3 (ck666) and formin homology 2 domain (smifH2) to matrix nanotopography is only partially reduced. b. Corresponding images of cells treated with the formin inhibitor. Scale bar is 10 µm. Green, vinculin; red, F-actin. c. Corresponding images for non-transfected cells (blank) or transfected with α-actinin siRNA1. Scale bar is 10 µm. Green, α-actinin; red, F-actin. d. Cell response to matrix nanotopography after α-actinin knock down is only partially reduced (α-Act-1 and -2 are two different siRNA against α-actinin; N.T., non-targeting).Error bars are s.e.m., $n \geq 3$; at least 100 cells for each replicate for each condition; *, $P < 0.05$; n.s., not significant; see Supplementary Tables 8 and 9 for statistical analysis.

nanotopography and geometry significantly, implying an important role of the cytoskeleton in such sensing.

Interestingly, GEβ1 cells were not found to be impacted by the two inhibitors (Supplementary Fig. 10a/b) and their response to nanotopography was similar in all conditions tested, in treated and untreated cells.

To investigate the role of cytoskeletal contractility on nanotopography sensing, we used the inhibitor of myosin contractility, blebbistatin, and disrupted cytoskeletal assembly using the ROCK inhibitor Y27632 (Fig. 6a and b and Supplementary Figs. S5–7). Both inhibitors effectively disrupted the actin cytoskeleton of GEβ3 cells spreading on homogenous control substrates, although with no significant change in the total cell spreading area (but significant impact on cell morphologies). Cells spreading on nanofibres and exposed to these inhibitors became insensitive to the width of the fibres (Fig. 6a). Interestingly, we observed that, although focal adhesions of cells spreading on homogenous substrates rapidly disassembled upon exposure to these inhibitors, they persisted in the case of cells spreading on nanofibres (Fig. 6b). In addition, GEβ1 cells treated with these two inhibitors displayed comparable cell spreading (Supplementary Fig. 10c/d). This is consistent with the lower response to the nanotopography that these cells generally presented. In addition, treatment of GEβ3 cells with the cyclic peptide stabilising filamentous actin Jasplakinolide resulted in the formation of actin aggregates, the full disruption of dorsal and transverse stress fibres and the severe reduction of cell spreading, in particular on nanopatterns (Supplementary Fig. S8). Overall, cytoskeletal assembly and myosin-generated contractility, rather than focal adhesion assembly, appear as essential mediators of nanotopography sensing.

https://doi.org/10.1016/j.biomaterials.2019.119683

To further examine the role of myosin contractility on nanotopography sensing and the formation of actin foci, we co-transfected GEβ3 cells with myosin-GFP and LifeAct, therefore enabling us to image the concerted dynamics of cytoskeleton assembly and myosin recruitment in cells spreading on nanopatterns (Fig. 6c). Myosin was associated with stress fibres and with the actin network of the lamella of cells spreading on homogenous substrates. Although myosin was still recruited at stress fibres in cells adhering to nanofibrous patterns, it also formed dense rings assembled around actin foci (Fig. 6c and Supplementary Videos 9–11). This resulting core-shell architecture persisted and migrated in conjunction with the rest of the surrounding actin network, sometimes merging with neighbouring acto-myosin rings. Disruption of these acto-myosin structures was found to occur via parallel disassembly of the actin foci and myosin ring. Such dynamics is strikingly reminiscent of that of actin supra-structures reported by Thery and Blanchoin, in which actin networks assembled from micropatterns of the nucleation promoting factor pWA quickly disassembled when exposed to myosin, resulting in the formation of actin foci [53]. Similarly, myosin was found to result in the breakdown of cortical actin networks assembled at supported lipid bilayers [54].

Therefore, myosin rings are found to form and contract actin foci, resulting in the destabilisation of the actin cytoskeleton and eventually partial retraction of actin-supporting adhesions. In order to explore the mechanism via which actin foci disassemble, we co-transfected cells with cofilin-GFP and LifeAct (Fig. 7a and b). Cofilin plays a central role in the regulation of actin dynamics and regulates actin disassembly, thereby controlling cell motility and invasiveness [55,56]. On homogenous substrates, cofilin was found to be relatively homogenously distributed throughout the cytoplasm, with sequestration at protrusions and at actin filaments following cell retraction (Supplementary Video 12). In cells spreading on nanopatterns, we observed that cofilin still localised at protrusions and retracting filaments, but also colocalised with actin foci (Fig. 7a and b and Supplementary Videos 13 and 14). The assembly and disassembly of actin and cofilin foci coincided both spatially and temporally, indicating that cofilin may play an important role in the destabilisation of actin foci and the regulation of nanotopography sensing. To test this hypothesis, we knocked down cofilin in GEβ3 cells before seeding on nanofibrous patterns (Fig. 7c and

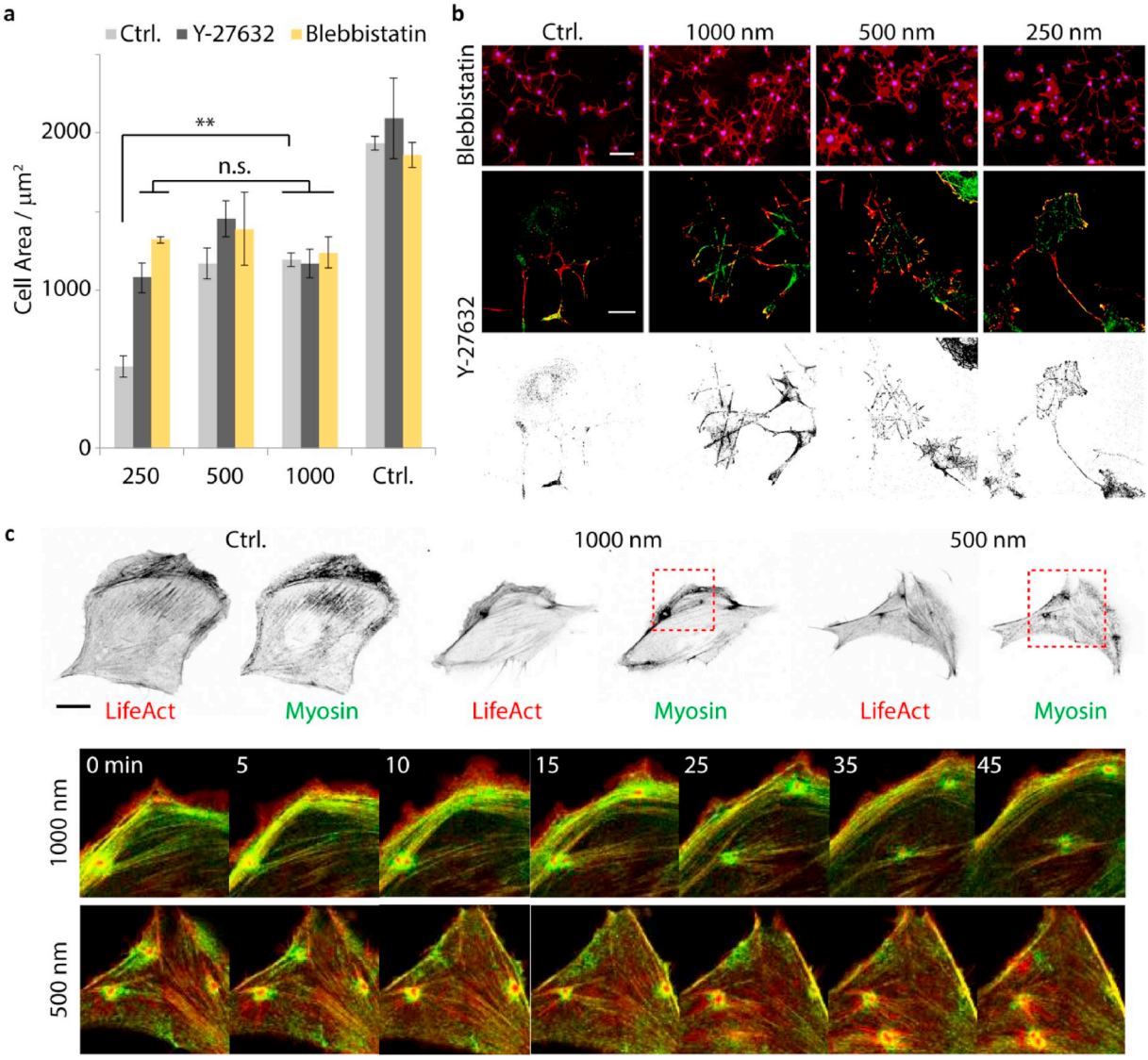

Fig. 6. Contractile myosin rings regulate the architecture of GEβ3 cell cytoskeleton and nanotopography sensing. a. Perturbation of the actin cytoskeleton disrupts nanotopography sensing. b. Cell adhesions persist for longer times in cells spreading on nanopatterns after disruption of their cytoskeleton. Scale bar for Blebbistatin is 100 µm and for Y-27632 is 20 µm. Green, vinculin; red, F-actin. c. Myosin rings form around actin foci. Time lapse imaging highlighting the dynamics of actin foci and myosin rings (see Supplementary Videos 9-11). Scale bar is 20 µm. Error bars are s.e.m., $n \geq 3$; at least 100 cells for each replicate for each condition; **, $P < 0.01$; n.s., not significant; see Supplementary Table 10 for statistical analysis.

Supplementary Fig. 9). We observed that cells in which cofilin expression was reduced became insensitive to the nanopattern size and overall spread more than on homogenous substrates. This coincided with an important change in the shape of cells spreading on nanofibres.

4. Conclusion

Overall, our results demonstrate that nanotopography sensing is regulated by different molecular mechanisms than the sensing of substrate mechanics and that of ligand molecular distribution (Fig. 8), yet is particularly sensitive to the type of integrin heterodimers expressed. Although β1 expressing cells are relatively insensitive to nanopattern dimensions, at least in the range tested, β3 expressing cells are found to be particularly sensitive to nanofibre width. In addition, rather than directly regulating the assembly of focal adhesions, substrate nanotopography imposes boundaries that modulate the spatial organisation of the actin network and stress fibres. This results in local network instabilities, upon myosin-generated contractility, that lead to the local collapse of the actin network into foci, surrounded by a myosin ring. The local geometry of the actin network and associated changes in microfilament curvature, regulated by cofilin recruitment [51,57], result in the sequestration of cofilin at the foci and the disassembly of the actin network. Eventually, this results in cell retraction. Although actin foci are the most apparent structures that can be observed in videos of actin dynamics, it is also likely that similar events occur within the lamella and at membrane protrusion, but cannot be resolved from the normal cytoskeletal architecture. Therefore, we propose that nanotopography sensing is mediated by a long-range mechanism, through the microscale organisation of the actin network and that such geometry modulates its contractile mechanical stability. In addition, beyond the sensing of engineered extra-cellular matrices, such as the nanofibres presently studied, we propose that similar long-range sensing processes and network stability, regulated by myosin contractility, also control cell spreading and migration within 3D environments (where fibrillar matrices are often prevalent). This is consistent with observations of the importance of adhesion dynamics in sensing the local geometry of 3D matrices and their regulation via actin contractility [58] and we note that cofilin has been implicated in the regulation of cell protrusion and

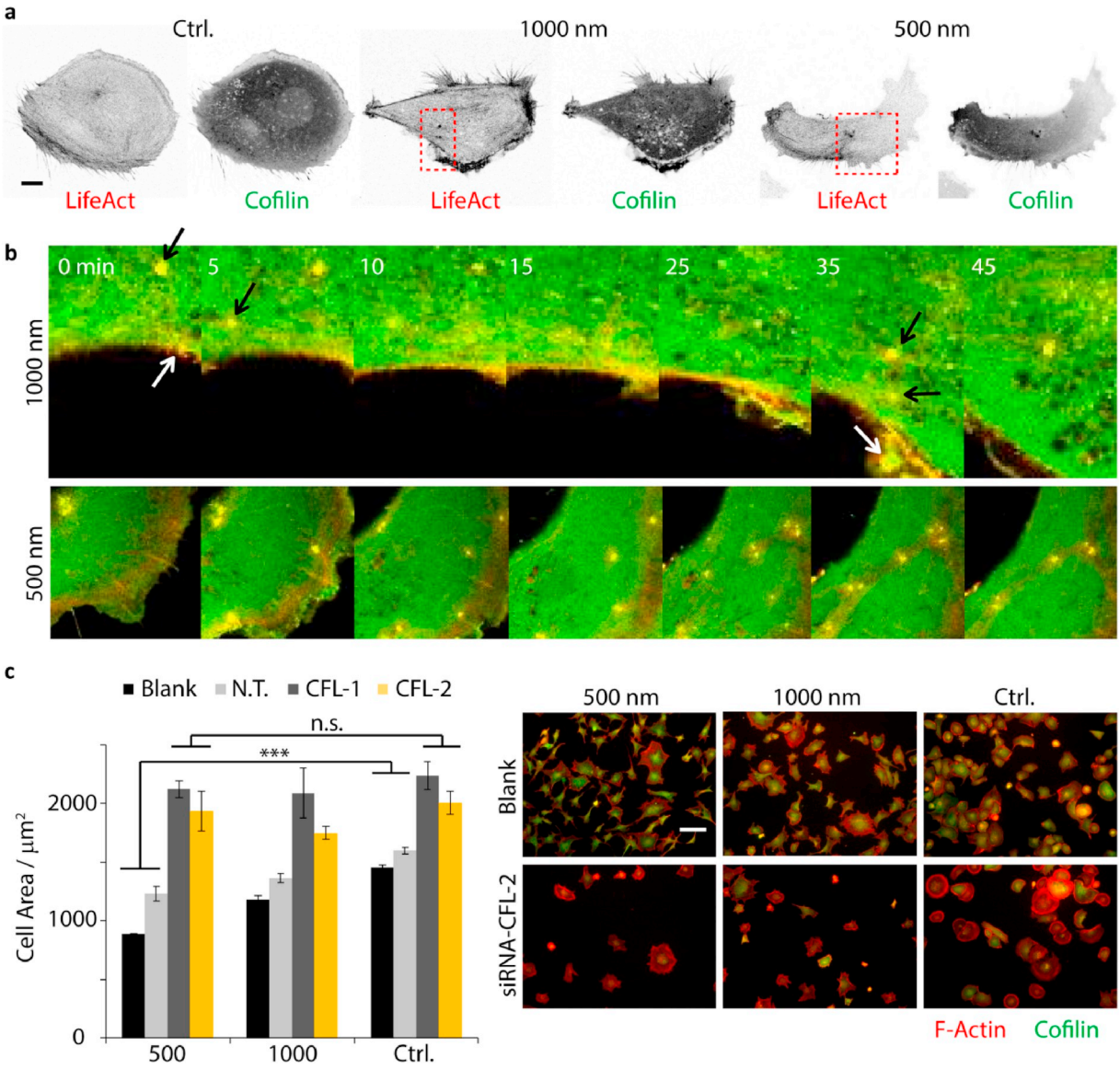

Fig. 7. Cofilin and actin disassembly orchestrates nanotopography sensing. a. Cofilin is recruited at actin foci formed in GEβ3 cells spreading on nanopatterns. Scale bar is 20 µm. b. Time lapse imaging of cells spreading on nanopatterns and clearly displaying colocalisation of cofilin at actin foci (see Supplementary Videos 12-14). c. Knock down of cofilin disrupts cell response to substrate nanotopography (CFL-1 and -2 are siRNA against cofilin; N.T., non-targeting). Scale bar is 100 µm. Error bars are s.e.m., $n \geq 3$; at least 100 cells for each replicate for each condition; ***, $P < 0.001$; n.s., not significant; see Supplementary Table 13 for statistical analysis.

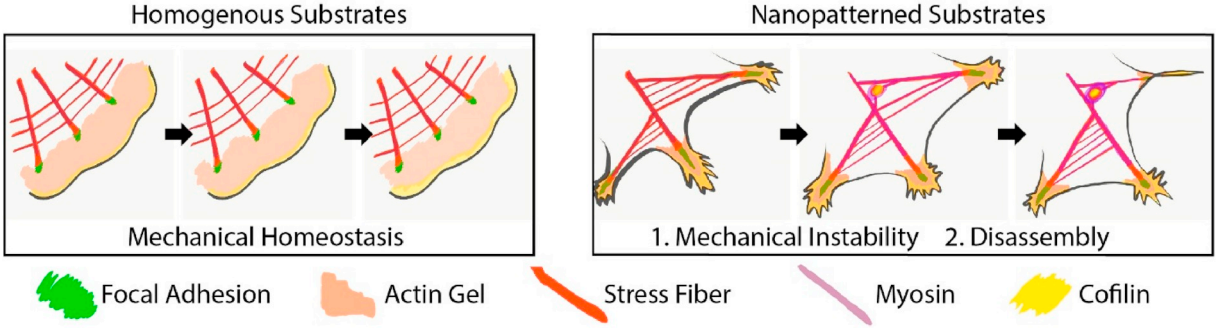

Fig. 8. Mechanism for the regulation of cell sensing of matrix nanotopography. The normal architecture of the cytoskeleton and its mechanical homeostasis is perturbed in cells spreading on nanopatterned substrates, where adhesions can only form along certain axis determined by the ECM geometry. This leads to the destabilisation of the actin cytoskeleton (but not focal adhesions), and the formation of contractile myosin rings and actin foci. Cofilin recruitment at these foci results in the disassembly of the cytoskeleton. Hence, the cytoskeleton and its complex dynamics appear as the primary sensor of matrix nanotopograpy, rather than focal adhesions.

motility in 3D matrices [59]. Questions also remain regarding the mechanisms that differentially regulate actin cytoskeleton assembly in β1 and β3 integrin-expressing cells, given that both of these transmembrane proteins form heterodimers that recruit similar adapter proteins.

Data availability

All data analysed during this study are included in this published article (and its supplementary information file). Other raw data required to reproduce these findings are available from the corresponding author on reasonable request.

Acknowledgment

We thank Prof. Arnoud Sonnenberg for sharing GE cell lines used in this study. Funding from the Institute of Bioengineering (Queen Mary, University of London; studentship for SDC) and from the European Research Council (ProLiCell, 772462) is gratefully acknowledged.

Appendix A. Supplementary data

Supplementary data to this article can be found online at https://doi.org/10.1016/j.biomaterials.2019.119683.

References

[1] J.T. Parsons, A.R. Horwitz, M.A. Schwartz, Cell adhesion: integrating cytoskeletal dynamics and cellular tension, Nat. Rev. Mol. Cell Biol. 11 (9) (2010) 633–643.
[2] F. Guilak, D.M. Cohen, B.T. Estes, J.M. Gimble, W. Liedtke, C.S. Chen, Control of stem cell fate by physical interactions with the extracellular matrix, Cell stem cell 5 (1) (2009) 17–26.
[3] J.D. Humphrey, E.R. Dufresne, M.A. Schwartz, Mechanotransduction and extracellular matrix homeostasis, Nat. Rev. Mol. Cell Biol. 15 (12) (2014) 802.
[4] H. Fujiwara, M. Ferreira, G. Donati, D.K. Marciano, J.M. Linton, Y. Sato, A. Hartner, K. Sekiguchi, L.F. Reichardt, F.M. Watt, The basement membrane of hair follicle stem cells is a muscle cell niche, Cell 144 (4) (2011) 577–589.
[5] M. Barczyk, S. Carracedo, D. Gullberg, Integrins, Cell Tissue Res. 339 (1) (2010) 269.
[6] Calderwood Harburger, Integrin signalling at a glance, J. Cell Sci. 122 (2009) 159–163.
[7] L.T. Senbanjo, M.A. Chellaiah, CD44: a multifunctional cell surface adhesion receptor is a regulator of progression and metastasis of cancer cells, Front. Cell Dev. Biol. 5 (2017) 18.
[8] S.-H. Kim, J. Turnbull, S. Guimond, Extracellular matrix and cell signalling: the dynamic cooperation of integrin, proteoglycan and growth factor receptor, J. Endocrinol. 209 (2) (2011) 139–151.
[9] P.M. Comoglio, C. Boccaccio, L. Trusolino, Interactions between growth factor receptors and adhesion molecules: breaking the rules, Curr. Opin. Cell Biol. 15 (5) (2003) 565–571.
[10] C.C. DuFort, M.J. Paszek, V.M. Weaver, Balancing forces: architectural control of mechanotransduction, Nat. Rev. Mol. Cell Biol. 12 (5) (2011) 308.
[11] L. Trichet, J. Le Digabel, R.J. Hawkins, S.R. Vedula, M. Gupta, C. Ribrault, P. Hersen, R. Voituriez, B. Ladoux, Evidence of a large-scale mechanosensing mechanism for cellular adaptation to substrate stiffness, Proc. Natl. Acad. Sci. U. S. A. 109 (18) (2012) 6933–6938.
[12] A.J. Engler, S. Sen, H.L. Sweeney, D.E. Discher, Matrix elasticity directs stem cell lineage specification, Cell 126 (4) (2006) 677–689.
[13] M.J. Dalby, N. Gadegaard, R. Tare, A. Andar, M.O. Riehle, P. Herzyk, C.D. Wilkinson, R.O. Oreffo, The control of human mesenchymal cell differentiation using nanoscale symmetry and disorder, Nat. Mater. 6 (12) (2007) 997–1003.
[14] R.J. McMurray, N. Gadegaard, P.M. Tsimbouri, K.V. Burgess, L.E. McNamara, R. Tare, K. Murawski, E. Kingham, R.O. Oreffo, M.J. Dalby, Nanoscale surfaces for the long-term maintenance of mesenchymal stem cell phenotype and multipotency, Nat. Mater. 10 (8) (2011) 637–644.
[15] E.A. Cavalcanti-Adam, A. Micoulet, J. Blummel, J. Auernheimer, H. Kessler, J.P. Spatz, Lateral spacing of integrin ligands influences cell spreading and focal adhesion assembly, Eur. J. Cell Biol. 85 (3–4) (2006) 219–224.
[16] J. Huang, S.V. Grater, F. Corbellini, S. Rinck, E. Bock, R. Kemkemer, H. Kessler, J. Ding, J.P. Spatz, Impact of order and disorder in RGD nanopatterns on cell adhesion, Nano Lett. 9 (3) (2009) 1111–1116.
[17] J.E. Gautrot, J. Malmstrom, M. Sundh, C. Margadant, A. Sonnenberg, D.S. Sutherland, The nanoscale geometrical maturation of focal adhesions controls stem cell differentiation and mechanotransduction, Nano Lett. 14 (7) (2014) 3945–3952.
[18] S. Di Cio, T.M. Bøggild, J. Connelly, D.S. Sutherland, J.E. Gautrot, Differential integrin expression regulates cell sensing of the matrix nanoscale geometry, Acta Biomater. 50 (2017) 280–292.
[19] A. Elosegui-Artola, X. Trepat, P. Roca-Cusachs, Control of Mechanotransduction by Molecular Clutch Dynamics, Trends in Cell Biology, (2018).
[20] R. Oria, T. Wiegand, J. Escribano, A. Elosegui-Artola, J.J. Uriarte, C. Moreno-Pulido, I. Platzman, P. Delcanale, L. Albertazzi, D. Navajas, Force loading explains spatial sensing of ligands by cells, Nature 552 (7684) (2017) 219.
[21] M. Schvartzman, M. Palma, J. Sable, J. Abramson, X. Hu, M.P. Sheetz, S.J. Wind, Nanolithographic control of the spatial organization of cellular adhesion receptors at the single-molecule level, Nano Lett. 11 (3) (2011) 1306–1312.
[22] E.K. Yim, E.M. Darling, K. Kulangara, F. Guilak, K.W. Leong, Nanotopography-induced changes in focal adhesions, cytoskeletal organization, and mechanical properties of human mesenchymal stem cells, Biomaterials 31 (6) (2010) 1299–1306.
[23] M.J. Dalby, N. Gadegaard, R.O. Oreffo, Harnessing nanotopography and integrin–matrix interactions to influence stem cell fate, Nat. Mater. 13 (6) (2014) 558.
[24] N.Q. Balaban, U.S. Schwarz, D. Riveline, P. Goichberg, G. Tzur, I. Sabanay, D. Mahalu, S. Safran, A. Bershadsky, L. Addadi, B. Geiger, Force and focal adhesion assembly: a close relationship studied using elastic micropatterned substrates, Nat. Cell Biol. 3 (5) (2001) 466–472.
[25] P.W. Oakes, Y. Beckham, J. Stricker, M.L. Gardel, Tension is required but not sufficient for focal adhesion maturation without a stress fiber template, J. Cell Biol. 196 (3) (2012) 363–374.
[26] C.K. Choi, M. Vicente-Manzanares, J. Zareno, L.A. Whitmore, A. Mogilner, A.R. Horwitz, Actin and alpha-actinin orchestrate the assembly and maturation of nascent adhesions in a myosin II motor-independent manner, Nat. Cell Biol. 10 (9) (2008) 1039–1050.
[27] I. Thievessen, P.M. Thompson, S. Berlemont, K.M. Plevock, S.V. Plotnikov, A. Zemljic-Harpf, R.S. Ross, M.W. Davidson, G. Danuser, S.L. Campbell, C.M. Waterman, Vinculin-actin interaction couples actin retrograde flow to focal adhesions, but is dispensable for focal adhesion growth, J. Cell Biol. 202 (1) (2013) 163–177.
[28] V. Schaufler, H. Czichos-Medda, V. Hirschfeld-Warnecken, S. Neubauer, F. Rechenmacher, R. Medda, H. Kessler, B. Geiger, J.P. Spatz, E.A. Cavalcanti-Adam, Selective binding and lateral clustering of α 5 β 1 and α v β 3 integrins: unraveling the spatial requirements for cell spreading and focal adhesion assembly, Cell Adhes. Migrat. 10 (5) (2016) 505–515.
[29] C. Gimond, A. Van Der Flier, S. Van Delft, C. Brakebusch, I. Kuikman, J.G. Collard, R. Fässler, A. Sonnenberg, Induction of cell scattering by expression of β1 integrins in β1-deficient epithelial cells requires activation of members of the rho family of GTPases and downregulation of cadherin and catenin function, J. Cell Biol. 147 (6) (1999) 1325–1340.
[30] E.H. Danen, J. van Rheenen, W. Franken, S. Huveneers, P. Sonneveld, K. Jalink, A. Sonnenberg, Integrins control motile strategy through a Rho–cofilin pathway, J. Cell Biol. 169 (3) (2005) 515–526.
[31] A.J. Zhu, I. Haase, F.M. Watt, Signaling via β1 integrins and mitogen-activated protein kinase determines human epidermal stem cell fate in vitro, Proc. Natl. Acad. Sci. 96 (12) (1999) 6728–6733.
[32] P. Roca-Cusachs, N.C. Gauthier, A. del Rio, M.P. Sheetz, Clustering of α5β1 integrins determines adhesion strength whereas αvβ3 and talin enable mechanotransduction, Proc. Natl. Acad. Sci. U.S.A. 106 (38) (2009) 16245–16250.
[33] H.B. Schiller, M.-R. Hermann, J. Polleux, T. Vignaud, S. Zanivan, C.C. Friedel, Z. Sun, A. Raducanu, K.-E. Gottschalk, M. Théry, M. Mann, R. Fässler, β1- and αv-class integrins cooperate to regulate myosin II during rigidity sensing of fibronectin-based microenvironments, Nat. Cell Biol. 15 (6) (2013) 625–636.
[34] J.E. Gautrot, B. Trappmann, F. Oceguera-Yanez, J. Connelly, X. He, F.M. Watt, W.T.S. Huck, Exploiting the superior protein resistance of polymer brushes to control single cell adhesion and polarisation at the micron scale, Biomaterials 31 (2010) 5030–5041.
[35] E.H.J. Danen, P. Sonneveld, C. Brakebusch, R. Fassler, A. Sonnenberg, The fibronectin-binding integrins α5β1 and αvβ3 differentially modulate RhoA-GTP loading, organization of cell matrix adhesions, and fibronectin fibrillogenesis, J. Cell Biol. 159 (6) (2002) 1071–1086.
[36] C. Gimond, A. Van Der Flier, S. Van Delft, C. Brakebusch, I. Kuikman, J.G. Collard, R. Fassler, A. Sonnenberg, Induction of cell scattering by expression of β1 integrins in β1-deficient epithelial cells requires activation of members of the rho family of GTPases and downregulation of cadherin and catenin function, J. Cell Biol. 147 (1999) 1325–1340.
[37] D.W. Zhou, T.T. Lee, S. Weng, J. Fu, A.J. García, Effects of substrate stiffness and actomyosin contractility on coupling between force transmission and vinculin–paxillin recruitment at single focal adhesions, Mol. Biol. Cell 28 (14) (2017) 1901–1911.
[38] D.W. Dumbauld, Ted T. Leea, Ankur Singha, Jan Scrimgeourb, Charles A. Gersbacha, Evan A. Zamir, Jianping Fud, Christopher S. Chene, Jennifer E. Curtisb, Susan W. Craigf, a.A.J. García, How vinculin regulates force transmission, Proc. Natl. Acad. Sci. 110 (24) (2013) 9788–9793.
[39] P. Monzo, Y.K. Chong, C. Guetta-Terrier, A. Krishnasamy, S.R. Sathe, E.K. Yim, W.H. Ng, B.T. Ang, C. Tang, B. Ladoux, Mechanical confinement triggers glioma linear migration dependent on formin FHOD3, Mol. Biol. Cell 27 (8) (2016) 1246–1261.
[40] B. Hetrick, M.S. Han, L.A. Helgeson, B.J. Nolen, Small molecules CK-666 and CK-869 inhibit actin-related protein 2/3 complex by blocking an activating conformational change, Chem. Biol. 20 (5) (2013) 701–712.
[41] T. Isogai, R. Van Der Kammen, M. Innocenti, SMIFH2 has effects on Formins and p53 that perturb the cell cytoskeleton, Sci. Rep. 5 (2015) 9802.
[42] D. Li, A.S. Sharili, J. Connelly, J.E. Gautrot, Highly stable RNA capture by dense cationic polymer brushes for the design of cytocompatible, serum-stable siRNA

delivery vectors, Biomacromolecules 19 (2) (2018) 606–615.
[43] J. Jacobelli, F.C. Bennett, P. Pandurangi, A.J. Tooley, M.F. Krummel, Myosin-IIA and ICAM-1 regulate the interchange between two distinct modes of T cell migration, J. Immunol. 182 (4) (2009) 2041–2050.
[44] B.K. Garvalov, K.C. Flynn, D. Neukirchen, L. Meyn, N. Teusch, X. Wu, C. Brakebusch, J.R. Bamburg, F. Bradke, Cdc42 regulates cofilin during the establishment of neuronal polarity, J. Neurosci. 27 (48) (2007) 13117–13129.
[45] E.H. Danen, P. Sonneveld, C. Brakebusch, R. Fässler, A. Sonnenberg, The fibronectin-binding integrins α5β1 and αvβ3 differentially modulate RhoA–GTP loading, organization of cell matrix adhesions, and fibronectin fibrillogenesis, J. Cell Biol. 159 (6) (2002) 1071–1086.
[46] L.B. Case, M.A. Baird, G. Shtengel, S.L. Campbell, H.F. Hess, M.W. Davidson, C.M. Waterman, Molecular mechanism of vinculin activation and nanoscale spatial organization in focal adhesions, Nat. Cell Biol. 17 (7) (2015) 880–892.
[47] J.D. Humphries, P. Wang, C. Streuli, B. Geiger, M.J. Humphries, C. Ballestrem, Vinculin controls focal adhesion formation by direct interactions with talin and actin, J. Cell Biol. 179 (5) (2007) 1043–1057.
[48] A. Carisey, R. Tsang, A.M. Greiner, N. Nijenhuis, N. Heath, A. Nazgiewicz, R. Kemkemer, B. Derby, J. Spatz, C. Ballestrem, Vinculin regulates the recruitment and release of core focal adhesion proteins in a force-dependent manner, Curr. Biol. 23 (4) (2013) 271–281.
[49] D.M. Cohen, H. Chen, R.P. Johnson, B. Choudhury, S.W. Craig, Two distinct head-tail interfaces cooperate to suppress activation of vinculin by talin, J. Biol. Chem. 280 (17) (2005) 17109–17117.
[50] J.D. Humphries, P. Wang, C. Streuli, B. Geiger, M.J. Humpries, C. Ballestrem, Vinculin controls focal adhesion formation by direct interactions with talin and actin, J. Cell Biol. 179 (2007) 1043–1057.
[51] T.M. Svitkina, G.G. Borisy, Arp2/3 complex and actin depolymerizing factor/cofilin in dendritic organization and treadmilling of actin filament array in lamellipodia, J. Cell Biol. 145 (5) (1999) 1009–1026.
[52] S. Tojkander, G. Gateva, P. Lappalainen, Actin stress fibers–assembly, dynamics and biological roles, J. Cell Sci. 125 (8) (2012) 1855–1864.
[53] A.C. Reymann, Rajaa Boujemaa-Paterski, Jean-Louis Martiel, Christophe Guérin, Wenxiang Cao, Harvey F. Chin, Enrique M. De La Cruz, Manuel Théry, L. Blanchoin, Actin network architecture can determine myosin motor activity, Science 336 (2012).
[54] K.A. Ganzinger, S.K. Vogel, J. Mucksch, P. Blumhardt, P. Schwille, Myosin-II activity generates a dynamic steady state with continuous actin turnover in a minimal actin cortex, J. Cell Sci. 132 (2018) jcs219899.
[55] M. Oser, J. Condeelis, The cofilin activity cycle in lamellipodia and invadopodia, J. Cell. Biochem. 108 (6) (2009) 1252–1262.
[56] M.-F. Carlier, V. Laurent, J. Santolini, R. Melki, D. Didry, G.-X. Xia, Y. Hong, N.-H. Chua, D. Pantaloni, Actin depolymerizing factor (ADF/cofilin) enhances the rate of filament turnover: implication in actin-based motility, J. Cell Biol. 136 (6) (1997) 1307–1322.
[57] A.-C. Reymann, C. Suarez, C. Guérin, J.-L. Martiel, C.J. Staiger, L. Blanchoin, R. Boujemaa-Paterski, Turnover of branched actin filament networks by stochastic fragmentation with ADF/cofilin, Mol. Biol. Cell 22 (14) (2011) 2541–2550.
[58] A.D. Doyle, N. Carvajal, A. Jin, K. Matsumoto, K.M. Yamada, Local 3D matrix microenvironment regulates cell migration through spatiotemporal dynamics of contractility-dependent adhesions, Nat. Commun. 6 (2015) 8720.
[59] R. Torka, F. Thuma, V. Herzog, G. Kirfel, ROCK signaling mediates the adoption of different modes of migration and invasion in human mammary epithelial tumor cells, Exp. Cell Res. 312 (19) (2006) 3857–3871.